REPORT No. 775

THE THEORY OF PROPELLERS

I—DETERMINATION OF THE CIRCULATION FUNCTION AND THE MASS COEFFICIENT FOR DUAL-ROTATING PROPELLERS

By THEODORE THEODORSEN

SUMMARY

Values of the circulation function have been obtained for dual-rotating propellers. Numerical values are given for four-, eight-, and twelve-blade dual-rotating propellers and for advance ratios from 2 to about 6. In addition, the circulation function has been determined for single-rotating propellers for the higher values of the advance ratio. The mass coefficient, another quantity of significance in propeller theory, has been introduced. This mass coefficient, which is actually the mean value of the circulation coefficient, expresses the effective area of the column of the medium acted upon by the propeller in terms of the propeller-disk area. Values of the mass coefficient, which have been determined directly by special measurements and also by integration of the circulation function, are given for the four-, eight-, and twelve-blade dual-rotating propellers. The mass coefficient has also been determined for several cases of single-rotating propellers, partly for the purpose of comparing such experimental values with theoretical results in the known range of low advance ratios and partly to extend the results to include a range of high advance ratios. The effect of stationary counter-vanes on the mass coefficient has also been determined for several cases of practical interest.

INTRODUCTION

CIRCULATION FUNCTION $K(x)$

In 1929 Goldstein (reference 1) succeeded in solving the problem of the ideal lift distribution of single-rotating propellers. Goldstein's work is restricted to the case of a light loading and also, in effect, to a small advance ratio. Numerical values given by Goldstein for the optimum circulation distribution are reproduced in table I and figure 1. Some additional values calculated by Kramer (reference 2) for higher advance ratios are given in table I and have been superimposed on the Goldstein results in figure 1. Numerical results by Lock and Yeatman (reference 3) for the four-blade propeller are reproduced in table II and figure 2. The parameter λ used in tables I and II is the tangent of the tip vortex angle in the ultimate wake

$$\lambda=\frac{1}{\pi}\frac{V+w}{nD}$$

where w is the rearward displacement velocity of the helical vortex surface at infinity. (A list of the symbols used throughout the paper is given in the appendix.) These data have been used for comparison with results contained in the present paper.

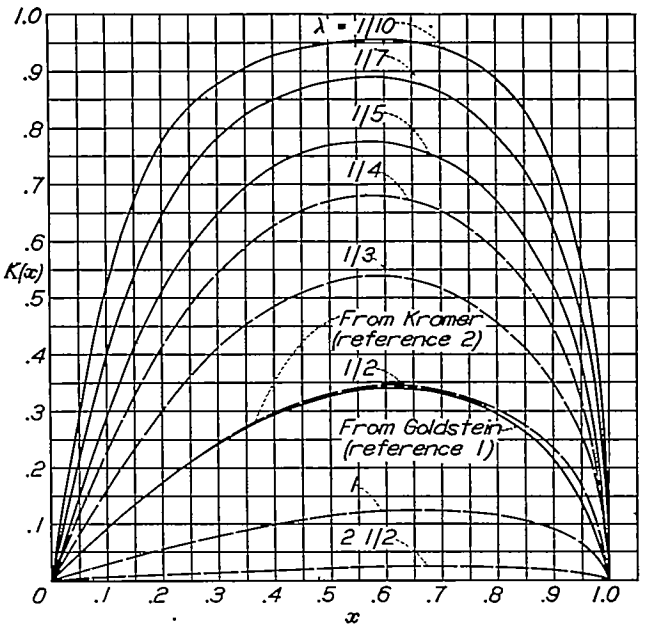

FIGURE 1.—The function $K(x)$ for several values of λ for two-blade propellers.

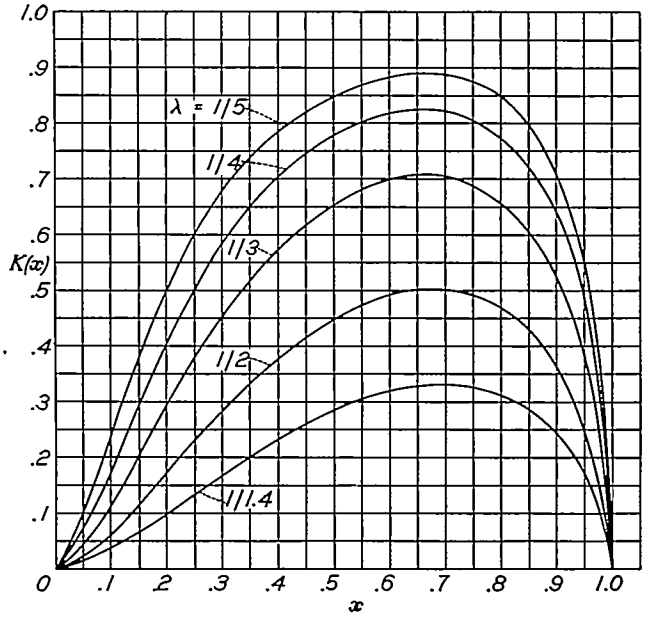

FIGURE 2.—The function $K(x)$ for several values of λ for four-blade propellers.

TABLE I

OPTIMUM CIRCULATION DISTRIBUTION FOR THE TWO-BLADE PROPELLER

Calculated by Goldstein (reference 1, p. 450)

x	$\lambda=\frac{1}{10}$	x	$\lambda=\frac{1}{7}$	x	$\lambda=\frac{1}{5}$	x	$\lambda=\frac{1}{4}$	x	$\lambda=\frac{1}{3}$	x	$\lambda=\frac{1}{2}$
0.020	0.126	0.029	0.126	0.040	0.124	0.050	0.120	0.067	0.111	0.100	0.092
.040	.245	.057	.245	.080	.240	.100	.232	.133	.213	.200	.175
.060	.352	.086	.351	.120	.344	.150	.331	.200	.303	.300	.243
.080	.445	.114	.443	.160	.434	.200	.418	.267	.379	.400	.295
.100	.526	.143	.523	.200	.511	.250	.489	.333	.440	.500	.329
.120	.593	.171	.590	.240	.575	.300	.548	.400	.485	.600	.341
.140	.650	.200	.646	.280	.626	.350	.592	.467	.514	.700	.331
.160	.698	.229	.694	.320	.669	.400	.628	.533	.533	.800	.295
.180	.738	.257	.732	.360	.704	.450	.654	.600	.537	.900	.220
.200	.772	.286	.766	.400	.731	.500	.670	.667	.525	----	-----
.250	.836	.357	.826	.500	.770	.625	.676	.833	.427	----	-----
.280	----	----	----	----	----	----	----	.933	.303	----	-----
.300	.878	.429	.863	.600	.775	.750	.621	----	----	----	-----
.350	.908	.500	.884	.700	.747	.875	.486	----	----	----	-----
.380	----	----	----	----	----	.950	.334	----	----	----	-----
.400	.927	.571	.890	.800	.671	----	----	----	----	----	-----
.450	.940	.643	.882	.900	.519	----	----	----	----	----	-----
.480	----	----	----	.960	.351	----	----	----	----	----	-----
.500	.950	.714	.858	----	----	----	----	----	----	----	-----
.600	.955	.857	.717	----	----	----	----	----	----	----	-----
.650	----	.929	.554	----	----	----	----	----	----	----	-----
.680	----	.971	.376	----	----	----	----	----	----	----	-----
.700	.941	----	----	----	----	----	----	----	----	----	-----
.800	.890	----	----	----	----	----	----	----	----	----	-----
.900	.738	----	----	----	----	----	----	----	----	----	-----
.950	.569	----	----	----	----	----	----	----	----	----	-----
.980	.388	----	----	----	----	----	----	----	----	----	-----

Calculated by Kramer (reference 2, p. 23)

x	$\lambda=\frac{1}{4}$	$\lambda=\frac{1}{3}$	$\lambda=\frac{1}{2}$	$\lambda=1.0$	$\lambda=2.5$
0.1	0.232	0.164	0.0319	0.0283	0.00494
.2	.418	.303	.1758	.0352	.00974
.3	.548	.412	.246	.0795	.01415
.4	.629	.486	.297	.0999	.01806
.45	.655	.510	----------	.1082	.01976
.5	.671	.528	.331	.1155	.02124
.6	.679	.540	.345	.1239	.02342
.7	.654	.517	.338	.1243	.02423
.75	.623	.493	.325	.1213	.02396
.8	.580	.457	.305	.1156	.02310
.85	.528	.413	.276	.1081	.02147
.9	.449	.351	.235	.0919	.0187
.925	.395	.311	----------	.0817	.0168
.95	.329	.260	.173	.0687	.0141
.975	-------	.190	----------	.0497	.0103

TABLE II

OPTIMUM CIRCULATION DISTRIBUTION FOR THE FOUR-BLADE PROPELLER

Calculated by Lock and Yeatman (reference 3)

x	$\lambda=\frac{1}{5}$	x	$\lambda=\frac{1}{4}$	x	$\lambda=\frac{1}{3}$	x	$\lambda=\frac{1}{2}$	x	$\lambda=\frac{1}{1.4}$
0.1200	0.300	0.150	0.299	0.0667	0.066	0.100	0.064	0.1429	0.061
.2000	.506	.250	.505	.1333	.179	.200	.173	.2857	.159
.3200	.706	.350	.649	.2000	.297	.300	.283	.4286	.249
.4000	.786	.400	.702	.2667	.405	.400	.377	.5714	.310
.5000	.848	.450	.744	.3333	.497	.500	.449	.7143	.329
.5600	.871	.500	.776	.4000	.572	.600	.492	.7857	.317
.6000	.881	.625	.821	.4667	.630	.700	.501	.8571	.282
.7000	.887	.700	.821	.5333	.672	.800	.469	.9286	.213
.7600	.872	.750	.806	.6000	.698	.900	.370	-------	-------
.8000	.850	.875	.689	.6667	.706	-----	-----	-------	-------
.9000	.714	.950	.488	.8333	.627	-----	-----	-------	-------
.9600	.503	-----	-----	.9333	.445	-----	-----	-------	-------

It should be emphasized that a distinction has been made between dimensions and conditions of the slipstream at the propeller and those in the ultimate wake, a distinction that does not occur in the treatment of lightly loaded propellers. The present paper is concerned exclusively with conditions in the ultimate wake; in fact, it can be shown that thrust, torque, and efficiency are all uniquely given as functions of the ultimate wake only, no knowledge of the propeller being necessary except for purposes of actual design. It should be pointed out that both the diameter and the advance angle of the ultimate helix are different from the values at the propeller, the diameter being smaller and the advance ratio larger. It can be shown that the distribution function depends on the advance angle only. The ideal distribution function is therefore identical for light and heavy loadings provided both refer to identical helix angles in the ultimate wake.

In figures 1 and 2 the quantity $K(x)$ is a characteristic function related to the circulation $\Gamma(x)$ along the blade as follows:

$$K(x)\equiv\frac{p\Gamma\omega}{2\pi(V+w)w}$$

where Γ is the potential difference across the helix surface at a radius x, p is the number of blades, and ω is the angular velocity of the propeller. The quantity

$$w\frac{V+w}{p\frac{\omega}{2\pi}}$$

is the potential drop for a velocity w through a length

$$\frac{H}{p}=\frac{V+w}{p\frac{\omega}{2\pi}}$$

which is the axial distance between two successive vortex sheets. Each sheet has $\frac{\omega}{2\pi}$ turns corresponding to a time of 1 second and there are p separate sheets corresponding to p blades. The quantity $K(x)$ is thus the nondimensional expression for the potential drop across the surface of discontinuity as a fraction of the available drop in the direction of the helix axis.

It should be noted that the coefficient $K(x)$ differs from the Goldstein coefficient

$$\frac{p\Gamma\omega}{2\pi Vw}$$

in which the velocity w has been disregarded in comparison with the advance velocity V. The coefficients are identical if referred to the same helix angle of the ultimate wake.

MASS COEFFICIENT κ

A significant coefficient, which will be termed the mass coefficient κ and which may be shown to be one of the basic parameters in the propeller theory, is now introduced. It is given here merely by definition

$$\kappa\equiv 2\int_0^1 K(x)x\,dx$$

where x is the radius and the integral is taken from $x=0$ to $x=1$. By inspection it is noted that κ is really the mean value of the coefficient $K(x)$ over the disk area. If $K(x)\equiv 1$, then $\kappa=1$, which is the limiting value of κ.

A physical interpretation of κ is interesting. It is possible to show that κ represents the effective cross-section of the column of the medium "pushed" by the propeller divided by the projected propeller-wake area. In other words, the propeller imparts the full interference velocity w to a column of air of cross-section κ per unit area of the ultimate propeller wake. The diameter of such a column is therefore $\sqrt{\kappa}$ for a propeller wake of unit diameter. Although mathematical refinements will not be considered in the present paper, this physical interpretation should suffice to indicate the nature of the coefficient and the designation adopted. It will be shown herein that the coefficient κ is readily obtained by direct measurements, to be described later.

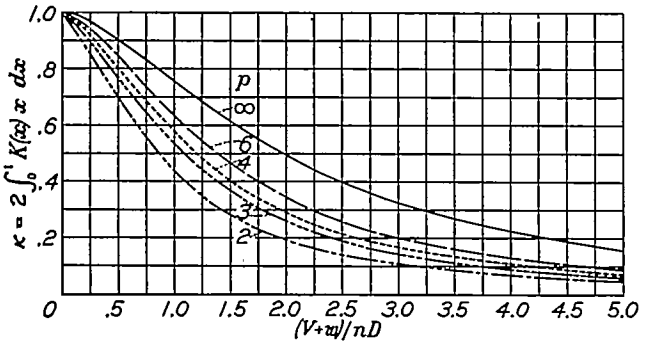

FIGURE 3.—Mass coefficient κ against $\frac{V+w}{nD}$ for various numbers of blades for single-rotating propellers.

Figure 3 shows curves for various values of the mass coefficient κ for the cases for which $K(x)$ is known—that is, for the single-rotating two- and four-blade propellers from tables I and II—as well as for the limiting case of an infinite number of blades. This latter case is readily obtained by integration. With

$$K(x)=\frac{x^2}{\lambda^2+x^2}$$

$$\kappa=2\int_0^1 \frac{x^2}{\lambda^2+x^2}x\, dx$$

is obtained or, after integration,

$$\kappa=1-\lambda^2\log\left(1+\frac{1}{\lambda^2}\right)$$

The curve for this equation is shown as the upper limit line in figure 3. Values for three- and six-blade propellers, which were calculated from data by Lock and Yeatman (reference 3), are also shown in figure 3. The curves in figure 3 are used later for comparison with data obtained in the present investigation.

ELECTRICAL METHOD AND EQUIPMENT FOR MEASURING $K(x)$ AND κ

DESCRIPTION

It is well known that the flow of electric currents in a field of uniform resistance is mathematically identical with the flow of a perfect fluid. The velocity potential may be perfectly reproduced by an electrical potential, provided the boundary conditions are identical.

For the present problem a direct measurement of the aerodynamic field behind a propeller presents insurmountable difficulties; in contradistinction, the electrical method of measurement is convenient and accurate and, in addition, permits the determination of local as well as integrated effects. The arrangement may, in fact, be considered a special calculating machine for solving the differential equation for given boundary conditions rather than a means for obtaining experimental solutions.

Since the ideal flow (far behind the propeller) is identical with the flow around a rigid helix moving at a constant velocity in the direction of its axis, the corresponding electric field is obtained very simply by inserting an insulating helix surface in a conducting liquid and applying a uniform field in the direction of the helix axis. The vessel confining the liquid is a long cylindrical shell, also of insulating material. The vessel is closed at both ends by copper end plates that are used as electrodes to apply the potential. The test-specimen helix is placed coaxially with the shell. The confining shell is considerably larger in diameter than the test helix.

Figure 4 is a photograph of the test setup for the direct determination of the mass coefficient κ. The cylinder on the right constitutes a dummy compensating resistance. The electrolyte used in these experiments consisted of tap water from the local water-supply system. The source of current was a 1000-cycle alternating-current generator producing a rather pure wave form at an available voltage of about 100 volts, which was applied to the electrodes. An exploring device consisting of a fine glass-insulated platinum wire with an exposed tip was used to determine the voltage at any point on the helix surface. This pickup device formed a part of a potentiometer circuit used in a Wheatstone bridge arrangement with a sensitive telephone as a zero indicator. When voltage readings were taken, no current passed through the telephone and the exploration wire. This type of measurement is inherently accurate; the error in the electrical measurements is estimated as not more than one part in 10,000.

Figure 5, also a photograph, shows the equipment used in the manufacture of the helix surfaces. The vertical insulated cylinder is an electrically heated oil tank. To the top center of this tank is attached a simple die or guiding device with a spiral slit through which the heated plastic sheet material is pulled at a uniform rate. A fan is used to supply cooling air at a uniform rate. With certain precautions an almost perfect helix is produced. Two models of single helix surfaces thus obtained are shown at the left and center in figure 6. A preliminary type of built-up model of laminated construction, which was abandoned as too inaccurate and expensive to build, is shown on the right in figure 6.

In figure 7(a) are shown examples of dual helix surfaces used for the main investigation. A four-blade dual-wake model is shown on the left and a six-blade dual-wake model is shown in the center. On the right is a four-blade single-rotation helix surface with four-blade "guide vanes." In figure 7(b) are other examples of high-order multiple dual-rotation wake models. Some additional examples of single-rotation wake models with guide vanes are shown in figure 8.

843110—50——4

The method of building the dual helix models is indicated in figure 9. Unit surfaces were cut from right- and left-handed helix surfaces and glued together to form a multiple dual helix. Fortunately these complex built-up dual models were needed only for determining the mass coefficient κ and did not have to be too accurate in detail.

For the dual-rotating-propeller field a significant property is to be noted: The field repeats itself not only along the axis but also circumferentially. A "unit cell" consisting of the helix surface between two successive lines of intersection is representative of the entire helix. It may be seen that the boundary condition is taken care of by inserting two insulating planes containing the axis and the two intersecting lines, respectively, and by using conducting end planes perpendicular to the axis which contain the same two intersecting lines. The vessel may therefore be given the form of an open V-shape tray with the electrodes at each end. The representative helix may be obtained simply by stretching a rubber membrane from one corner of the tray to the opposite corner at the other end. The membrane is equipped with stiff radial spokes and is securely clamped in place. It automatically assumes a spiral shape, the effects of gravity being of secondary order. The entire tray is arranged on a machine lathe with the helix axis along the center line and the exploring needle is attached to the carriage. This arrangement affords convenient reading of the voltage at any point on the spiral surface. In order to increase accuracy, the trays were made of considerable size, 6 to 10 feet long. By changing the length and the angle of the tray, all values of λ and the effect of the number of blades could be investigated.

In figures 10 and 11 are shown experimental setups for measuring the potential distribution $K(x)$. The connections leading to the exploring needle may be seen in figure 11.

Figures 12, 13, and 14 show the general arrangement for determination of the potential distribution on dual wake models. Figure 12 shows a unit cell for very low advance ratio. Note the V-shape test tank and the adjustable end plate to change the advance ratio. Note, also, the rubber membrane stretched between opposite corners. Figure 13 shows the arrangement for supporting the exploring needle. In figure 14 is finally shown the complete experimental setup for dual helix surfaces of very high pitch.

WALL, END, AND THICKNESS CORRECTIONS

The similarity between the electrical test method and the conventional wind-tunnel method may be extended also to include certain corrections. Obviously there is a correction that corresponds to the customary wall correction. This correction is readily ascertained by use of vessels of different

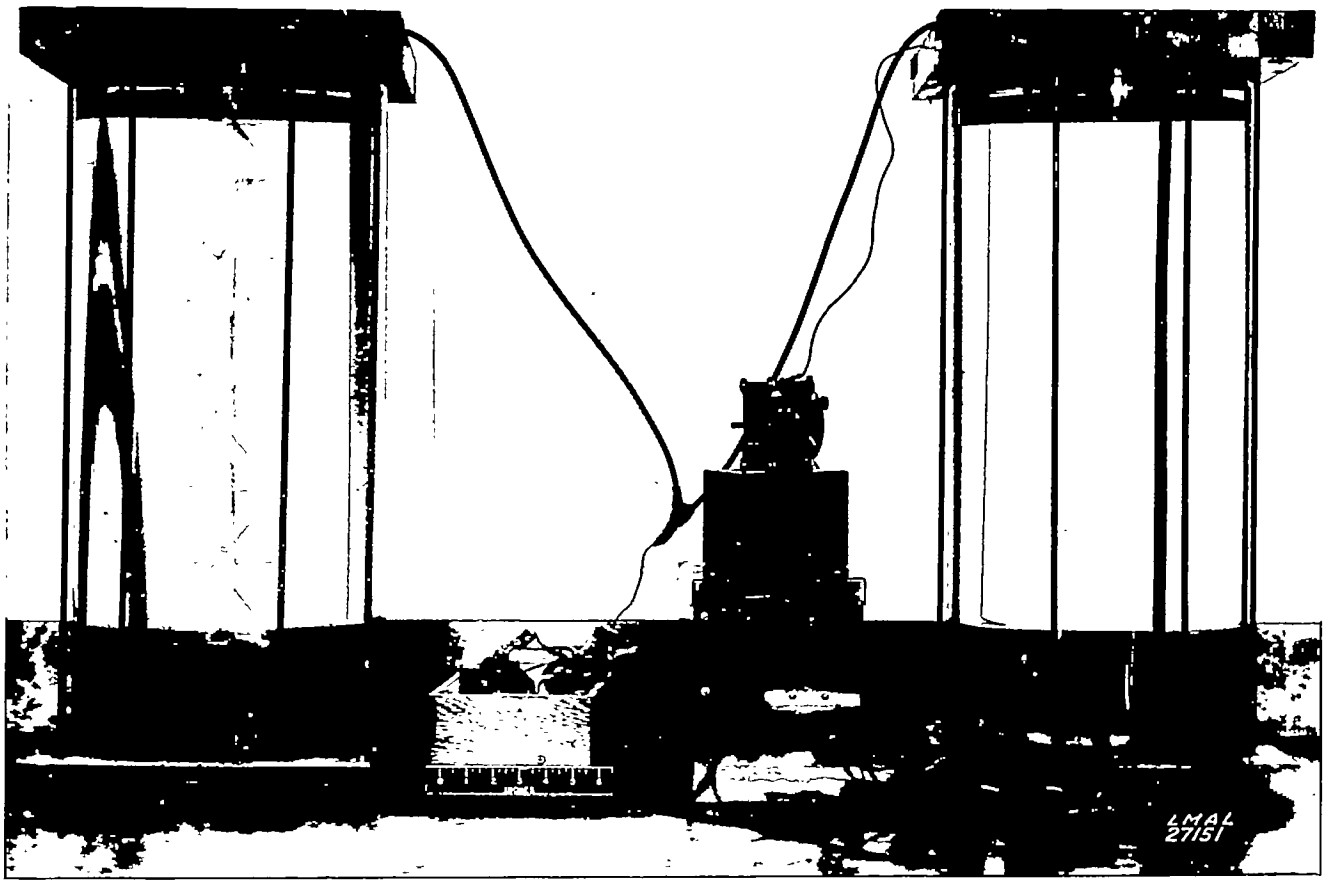

FIGURE 4.—Test setup for direct determination of the mass coefficient κ.

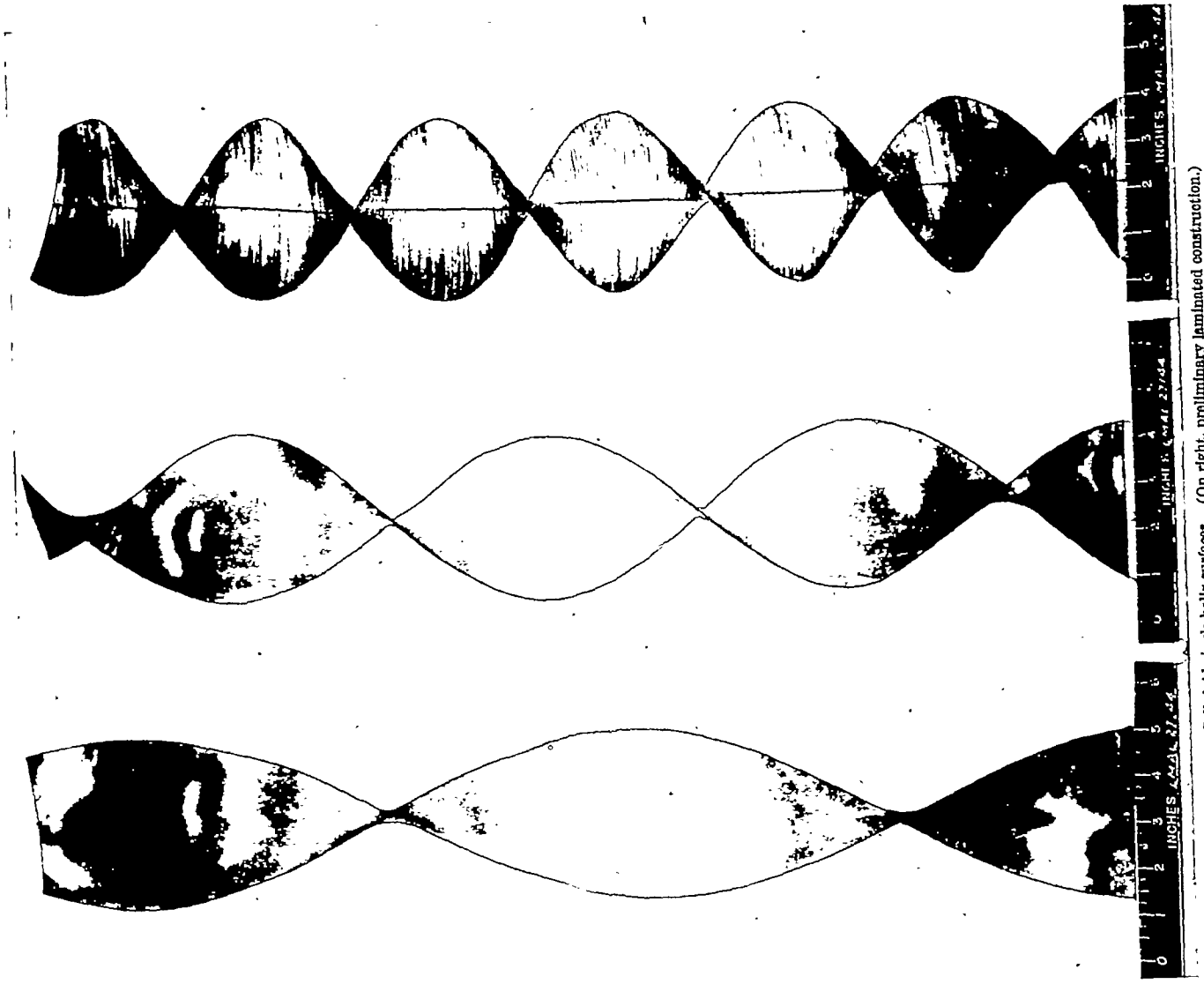

FIGURE 6.—Celluloid single helix surfaces. (On right, preliminary laminated construction.)

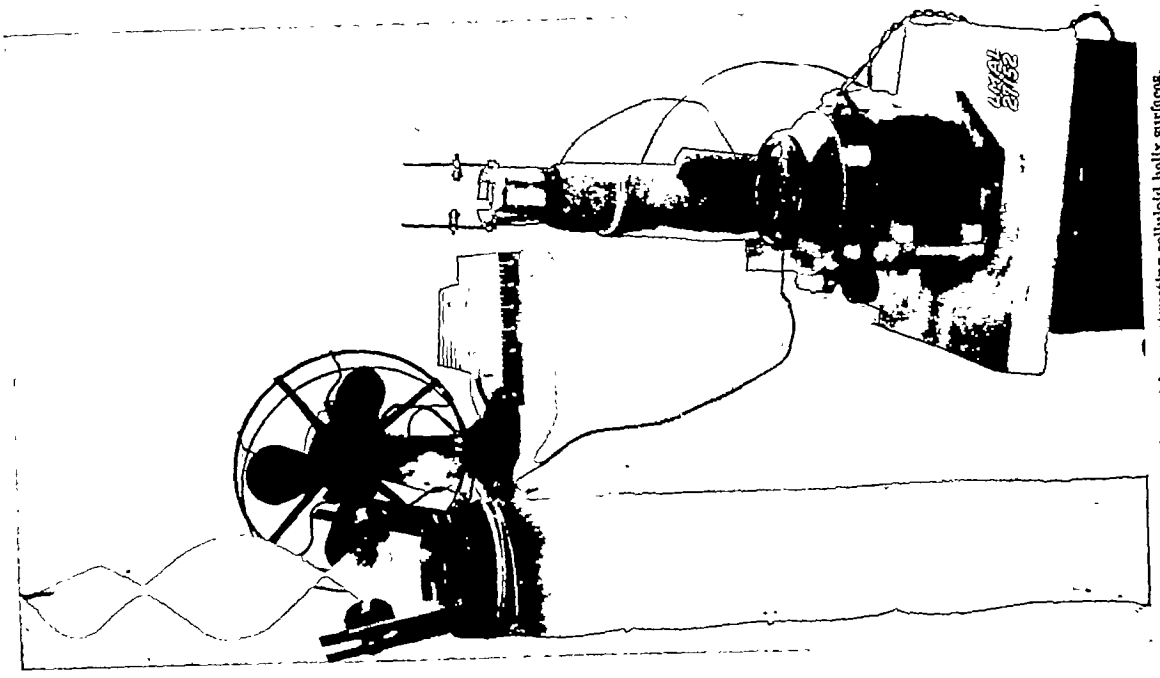

FIGURE 5.—Equipment for constructing celluloid helix surfaces.

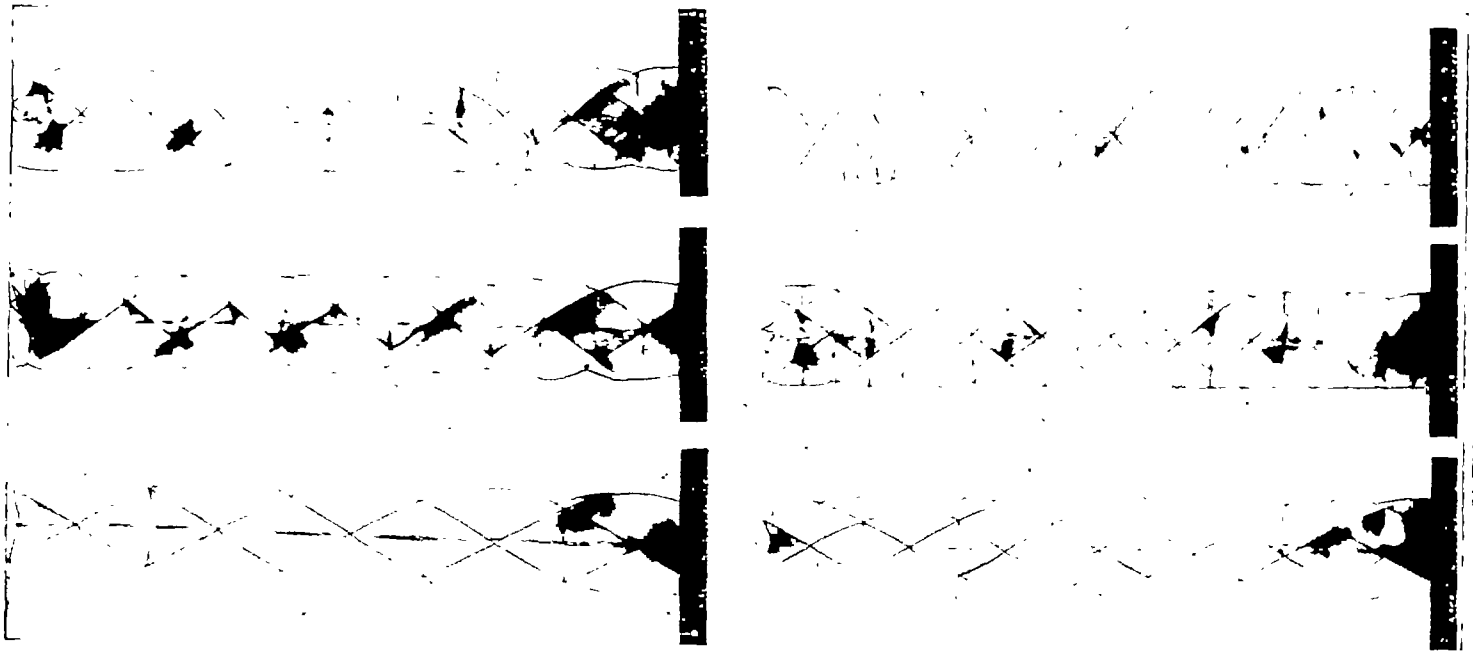

(b) High-order multiple blades, dual-rotation.

FIGURE 7.—Concluded.

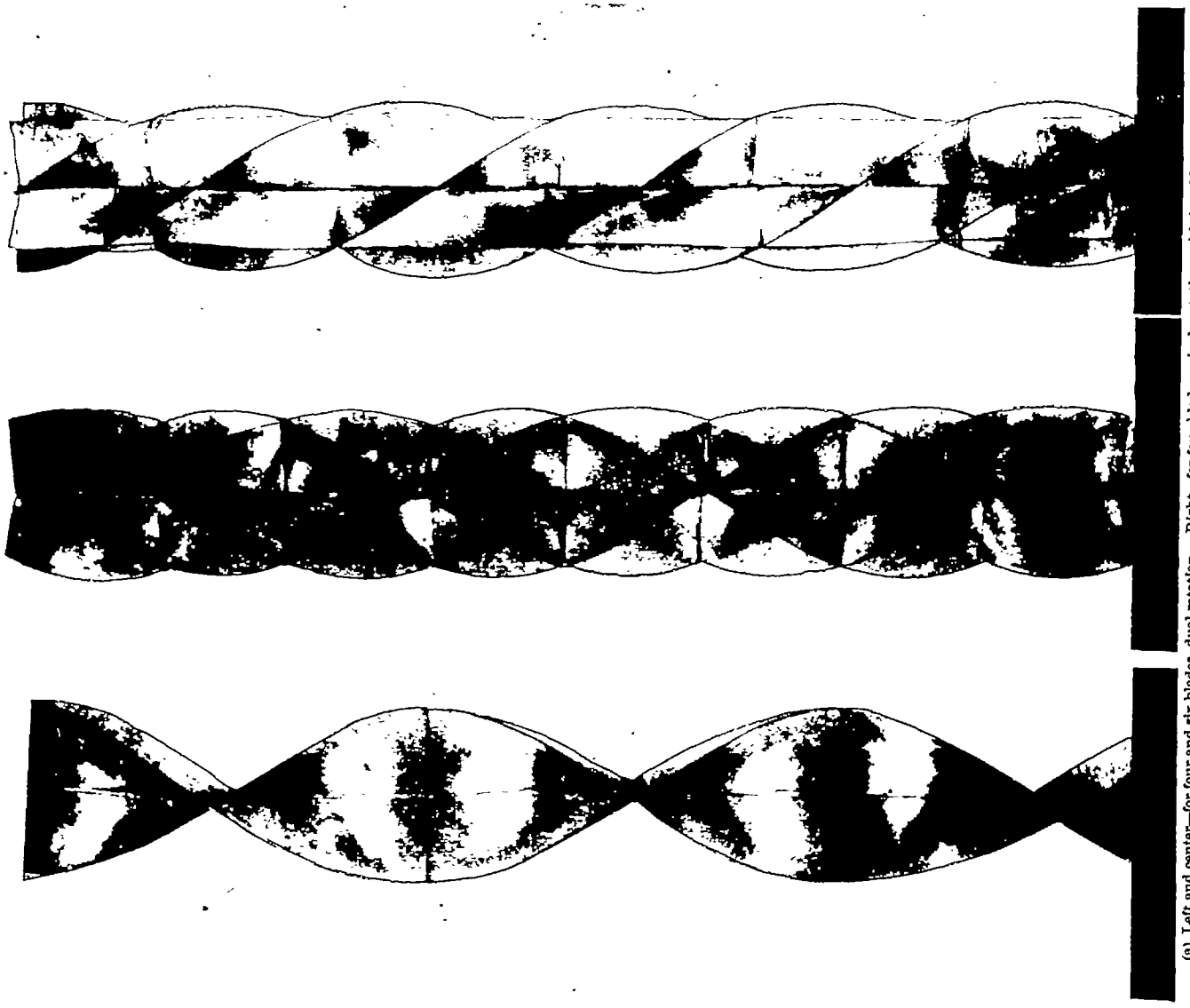

(a) Left and center—for four and six blades, dual-rotation. Right—for four blades, single-rotation, with four-blade guide vanes.

FIGURE 7.—Dual helix surfaces.

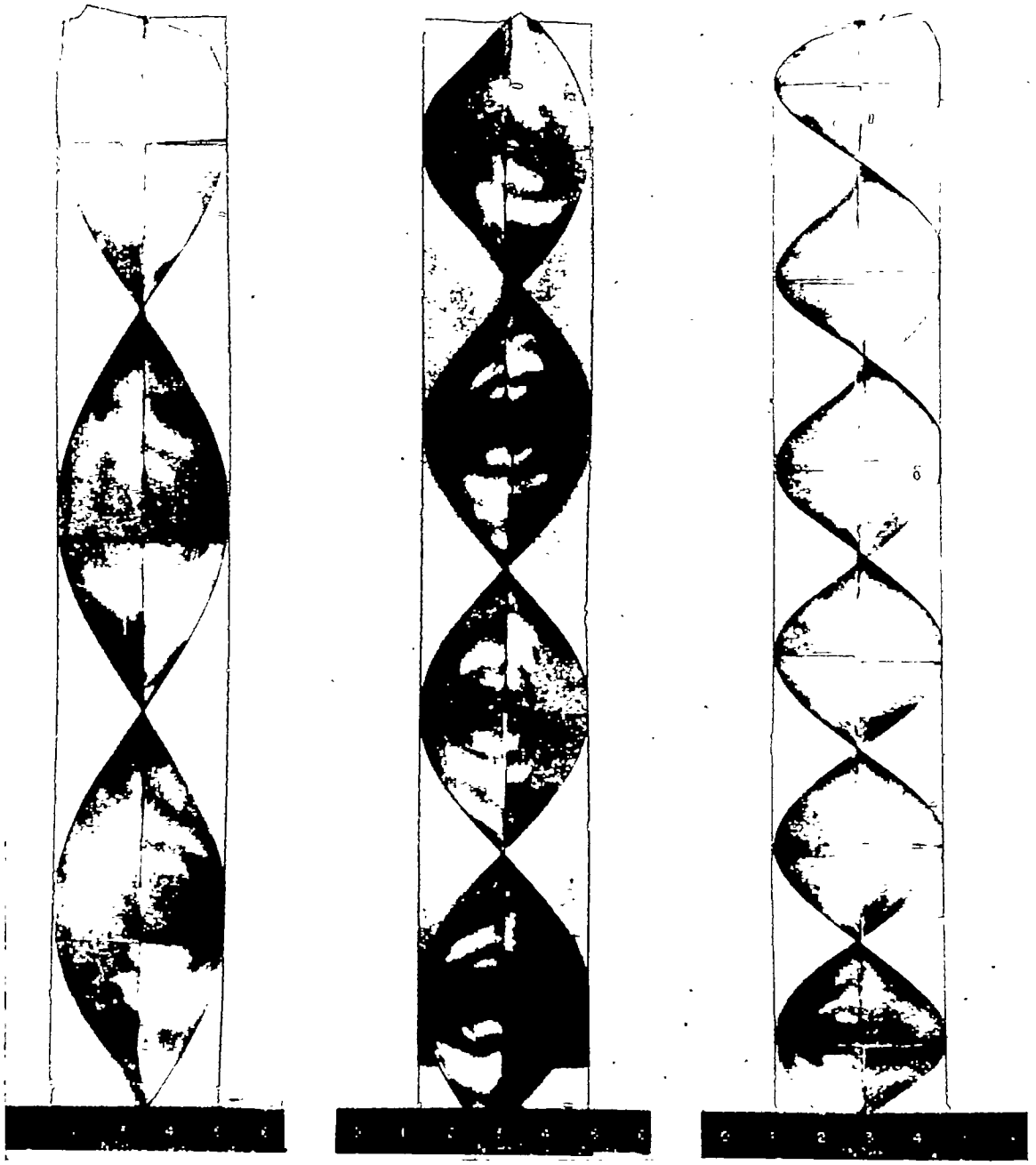

FIGURE 8.—Two-blade single-rotation helix surfaces with guide vanes.

diameters, a procedure that cannot be easily utilized in wind-tunnel practice. It should be noted further that the wall corrections are obtained with great accuracy since each reading by the electrical method is more precise than its aerodynamic counterpart. By using tube diameters about three times the diameter of the test spiral the error in the results was reduced to less than ½ percent.

A correction not appearing in aerodynamic practice is the end correction. This correction occurs only with single-rotating propellers and is therefore of minor importance in the present investigation. Dual-rotating propellers possess planes of constant potential perpendicular to their axes, and the ends therefore cause no difficulties. By cutting the dual helix at a plane of constant potential and by inserting a conducting end plate in the cylinder the boundary condition is satisfied. For single helix surfaces, tests on two lengths of the same helix must be used and the difference observed. This procedure was used to measure the mass coefficient κ. To measure the potential distribution $K(x)$ a long helix is required, the measurements to be made near the middle.

Another source of error exists for which the correction has been referred to as the thickness correction. This error results from the fact that the material of the helix sheet must have a finite thickness. This error may be determined by using sheets of two or more thicknesses. It is readily seen from theoretical considerations that approximately one-half the thickness of the sheet must be added to the diameter in order to obtain an equivalent infinitely thin sheet.

It should be mentioned finally that there is an error resulting from inaccuracies in the model vortex sheets. The error in $K(x)$ can be minimized by using mean values from a large number of readings over a considerable portion of the helix. Fortunately, there is no effect on the mass coefficient κ since this coefficient is a mean-value parameter.

PROOF THAT THE MASS COEFFICIENT κ IS THE BLOCKING EFFECT OF THE (INFINITELY LONG) HELIX SURFACE

The mass coefficient κ is obtained experimentally by measuring the change in resistance caused by the helix surface when inserted in the cylindrical container. On inserting the (infinitely long) helix in the container, the current between the end plates I_0 is decreased by a definite amount ΔI, and it can be proved that

$$\frac{\kappa F}{S}=\frac{\Delta I}{I_0}$$

or

$$\kappa=\frac{\Delta I}{I_0}\frac{S}{F}$$

where F is the projected cross section of the helix and S is the cross section of the cylindrical container.

By Green's theorem

$$\int_\sigma (U\nabla W-W\nabla U)d\sigma=\int_\tau (U\nabla^2 W-W\nabla^2 U)d\tau$$

If

$$\nabla^2 U=\nabla^2 W=0$$

it follows that

$$\int_\sigma (U\nabla W-W\nabla U)d\sigma=0$$

Let W be the distance z along the helix axis measured from a reference plane perpendicular to the axis; ∇W is therefore a unit vector in the direction z. Let U be the potential resulting from the applied voltage and the local gradient ∇U may be written

$$\nabla U=\frac{U_0}{L}\frac{i}{i_0}$$

Figure 9.—Steps in the construction of the more complicated helix surfaces.

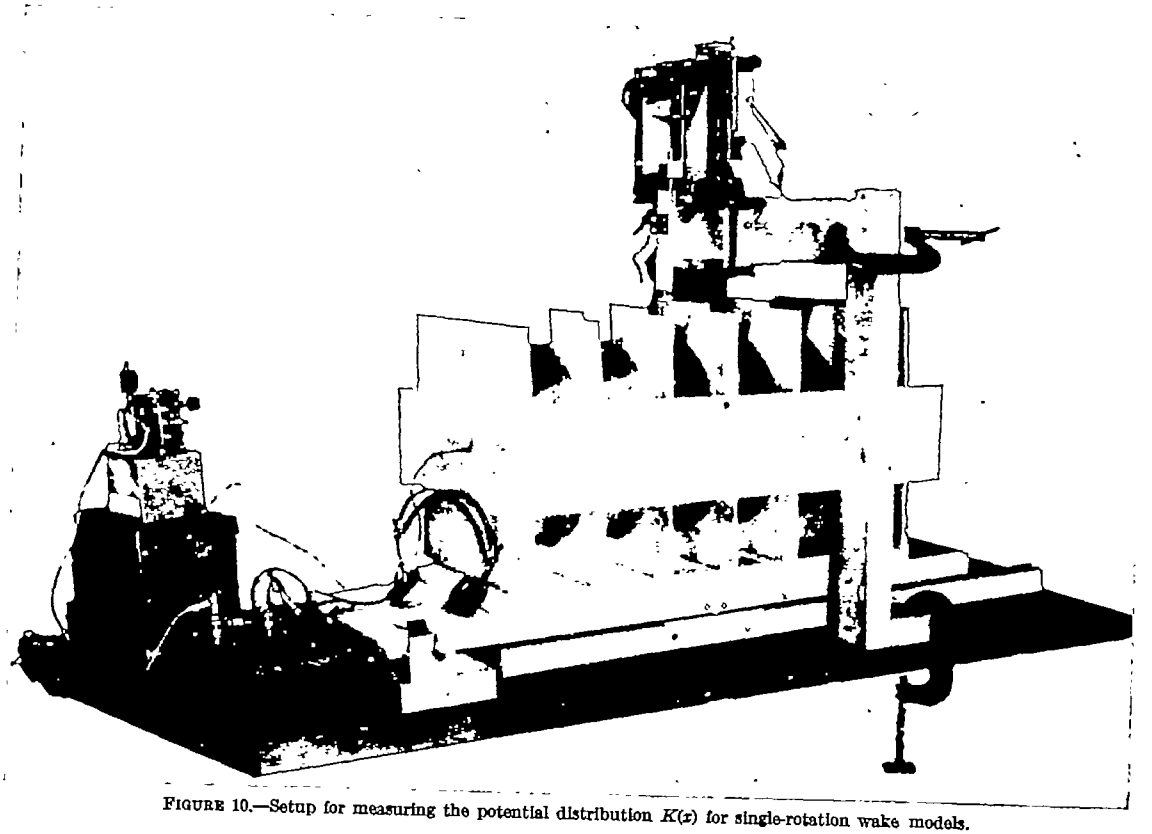

FIGURE 10.—Setup for measuring the potential distribution $K(x)$ for single-rotation wake models.

FIGURE 11.—Setup for measuring potential distribution $K(x)$ for single-rotation wake models, showing detail of exploring device.

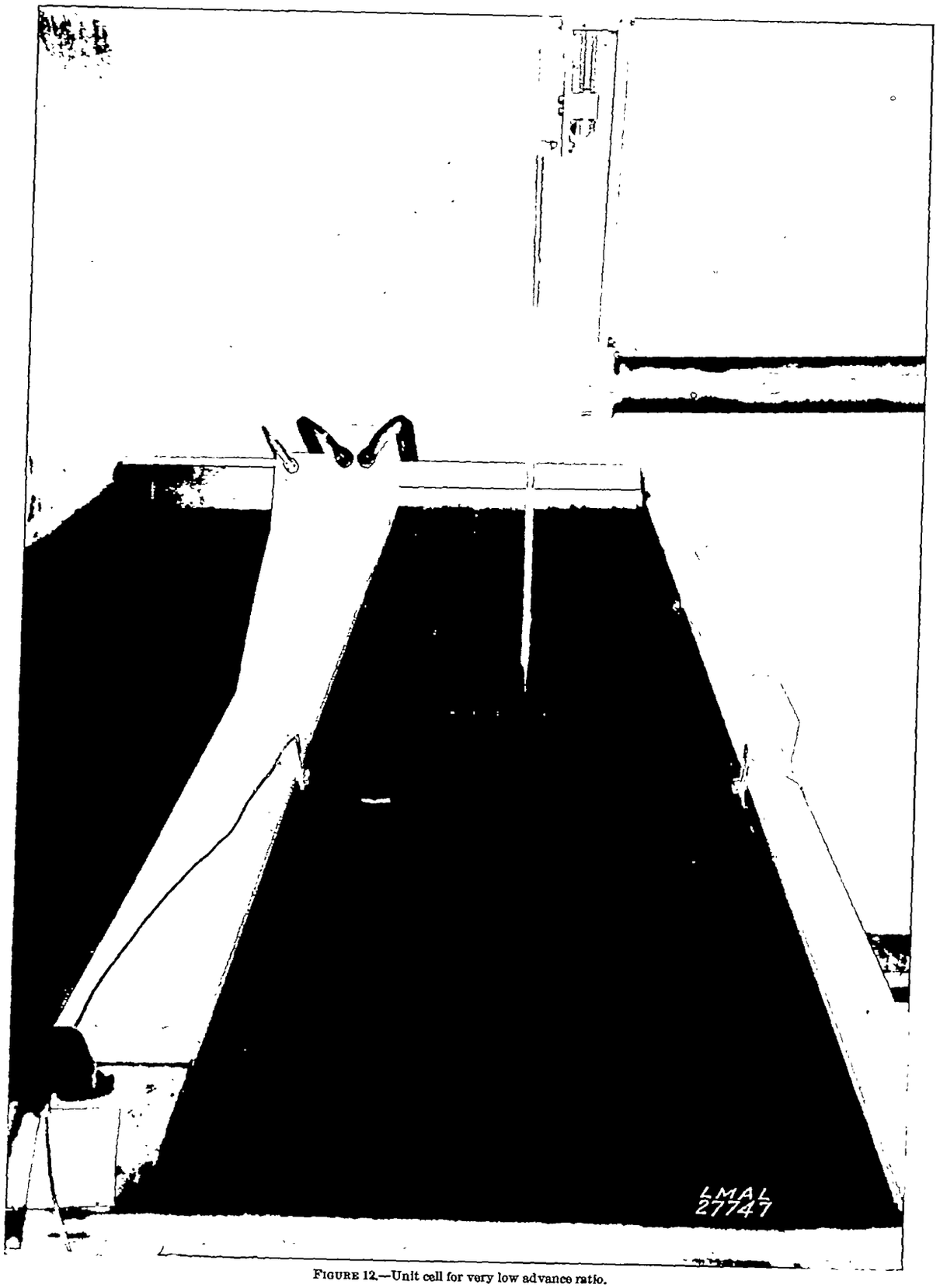

FIGURE 12.—Unit cell for very low advance ratio.

where U_0 is the constant voltage difference between the end plates, which are placed at an axial distance L apart, and i is the local current and i_0 the current at infinity. If the surface integrals for the entire enclosed helix surface A and the end surfaces S, respectively, are taken, the following relation is obtained

$$\int_A U\,dA_z = \int_S \left(U - z\frac{U_0}{L}\frac{i}{i_0}\right) dS$$

or

$$\frac{1}{U_0}\int_A U\,dA_z = \int_S \left(\frac{U}{U_0} - \frac{z}{L}\frac{i}{i_0}\right) dS$$

where the integrals are to be taken over both sides of the p helix surfaces and over both end plates. However,

$$\frac{1}{U_0}\int_A U\,dA_z$$

may be written in the form

$$\frac{pL}{U_0 H}\int (U_1 - U_2)\,dF$$

where the integral is taken over one turn of one helix for one side only, as $U_1 - U_2$ is the difference potential between the two sides of the sheet. The voltage drop per sheet is

$$\frac{U_0}{L}\frac{H}{p}$$

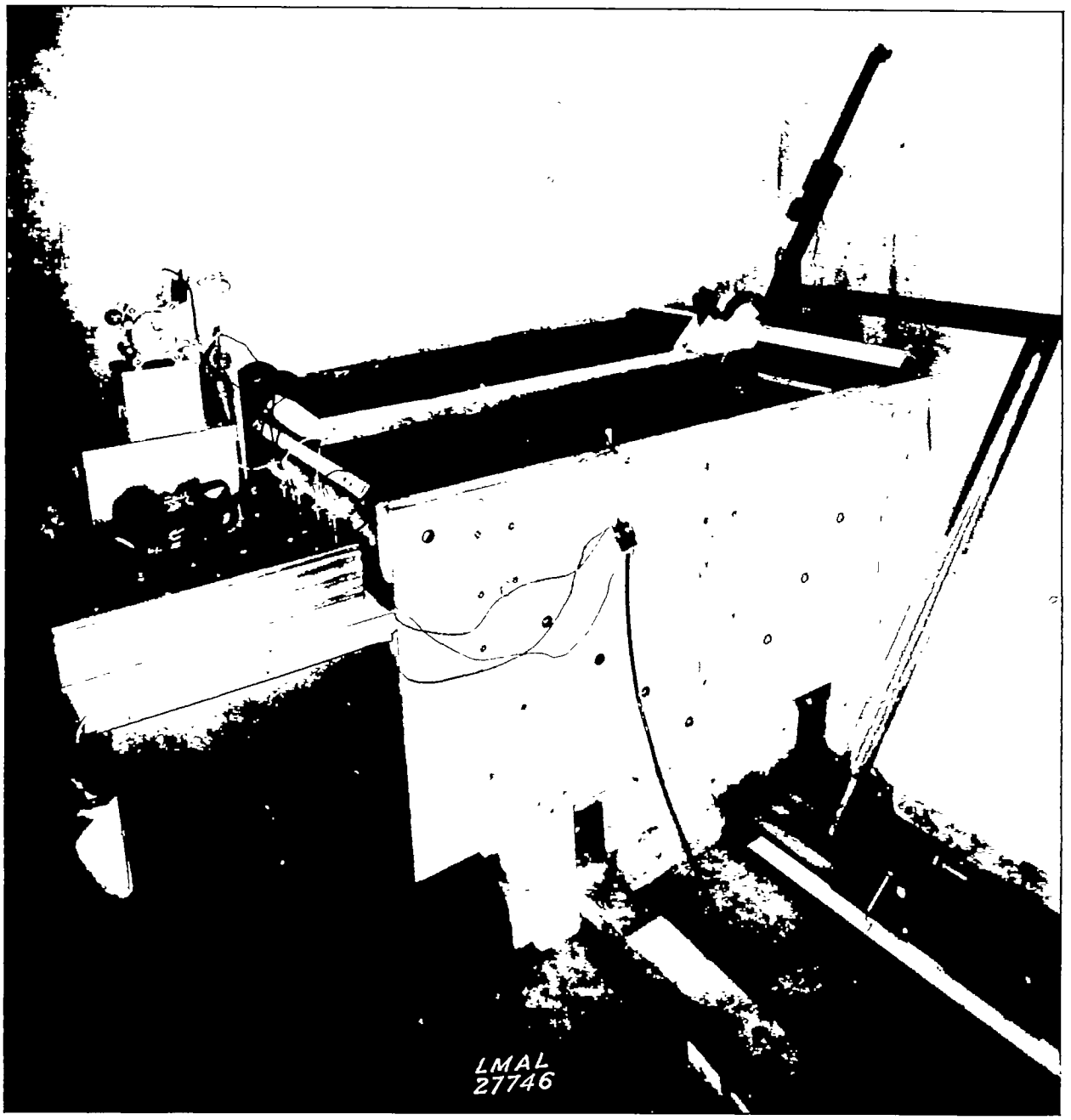

FIGURE 13.—Unit cell for very low advance ratio, showing arrangement of exploring device.

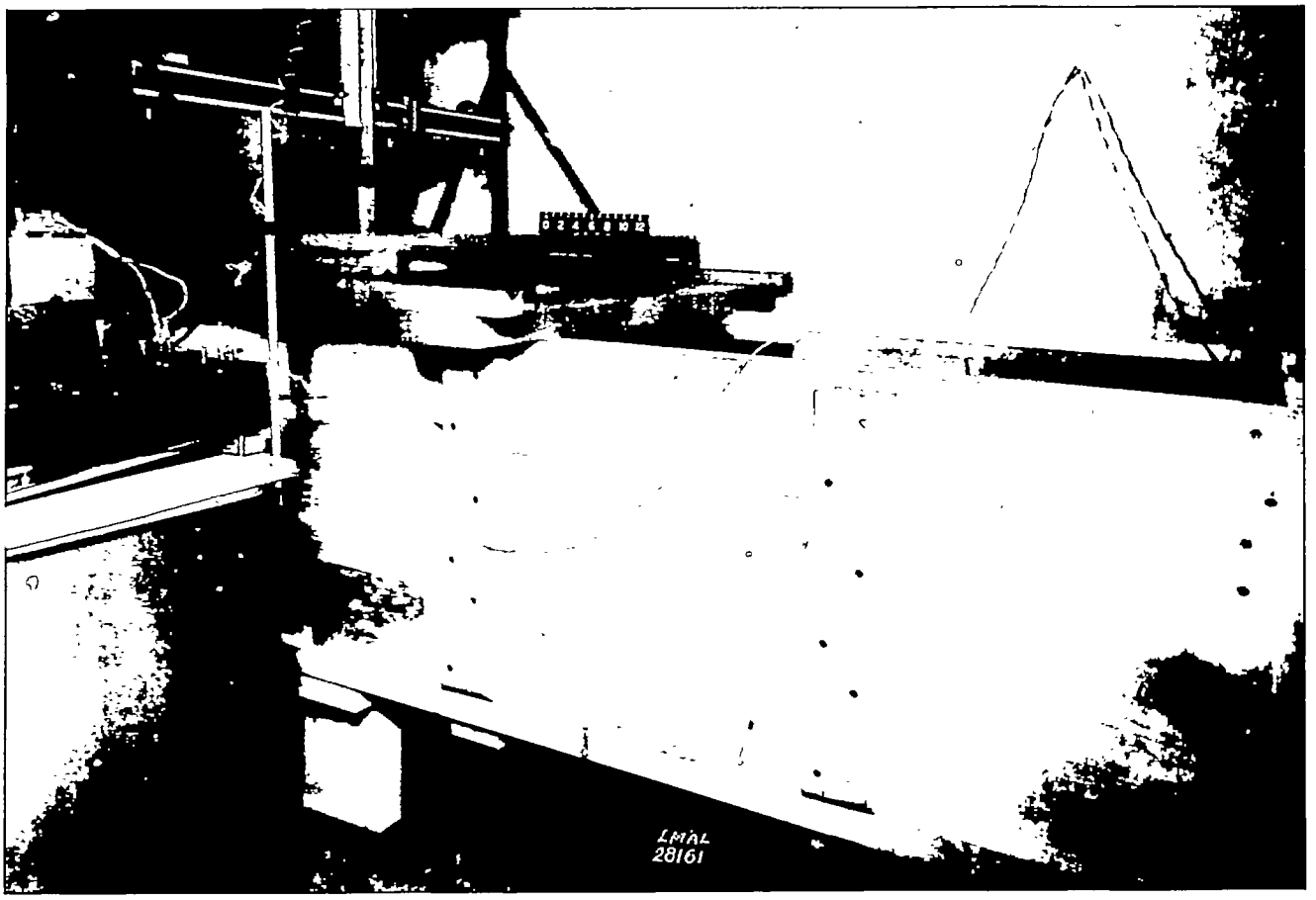

FIGURE 14.—Unit cell for high pitch.

By definition

$$K(x)=\frac{U_1-U_2}{\frac{U_0}{L}\frac{H}{p}}$$

Thus

$$\frac{1}{U_0}\int_1 U\,dA_2=\int_F K(x)\,dF=2F\int_0^1 K(x)x\,dx=\kappa F$$

Also,

$$\int_S\left(\frac{U}{U_0}-\frac{z}{L}\frac{i}{i_0}\right)dS=\int_S\left(1-\frac{i}{i_0}\right)dS=\frac{\Delta I}{I_0}S$$

and therefore

$$\frac{\kappa F}{S}=\frac{\Delta I}{I_0}$$

where I_0 is the total current between the end plates with a uniform gradient $\frac{U_0}{L}$ in the field.

EXPERIMENTAL DATA

MASS COEFFICIENT κ

Numerical values for the mass coefficient κ, obtained on dual-rotation wake models, are shown in figure 15. This chart is probably adequate for all practical purposes, as a large range of advance ratio has been covered. The designation used for the propellers comprises three digits: The first digit refers to the number of right-handed blades, the middle digit to the number of guide vanes, and the last digit to the number of left-handed blades—for instance, 3–0–3 represents a dual-rotating propeller with three right-handed and three left-handed blades. The highest number of blades tested was for a 6–0–6 or twelve-blade propeller.

As a matter of interest, it is very fortunate that the method and equipment could be tried out in all its ramifications on the known case of the Goldstein curve for a two-blade propeller. The Goldstein curve is the curve in figure 15 marked "Theoretical." The test points, which have been corrected for wall, thickness, and end effects, are shown. Except in a very few cases, the test points lie on the theoretical curve for the two-blade propellers. The somewhat lesser consistency in the cases of dual-rotating propellers is not due to inherent test inaccuracy but rather to a necessary limitation on time and equipment for making the models, performing the tests, and obtaining the corrections. The thickness correction for the high advance ratios is considerable. Note that three thicknesses have been used for many of the test points. A glance at one of the composite models shown in figure 7(b) will suffice to indicate the labor involved in producing the models. Each test point in figure 15 represents a different complete model; some fifty models thus are represented by the results shown. This number was necessary in order to include all propellers and all advance ratios of interest at present and in the future.

Results for single-rotation wake models with guide vanes are shown in figure 16 for two-, three-, and four-blade propellers, respectively. Such guide vanes are supposed to represent stationary vanes arranged immediately in front of

or behind the propeller to straighten the flow. It should be noted that the cases shown correspond to those of an ideal thrust distribution both on the propeller and on the guide vanes. The uppermost curve in each part of figure 16 is reproduced for purposes of comparison with the corresponding dual case.

DISTRIBUTION FUNCTION $K(x,\theta)$

The measured potential distributions on dual wake models are shown in figure 17. These tests were made on large-scale unit cells of the type described earlier. Figure 17 contains results on 2–0–2, 4–0–4, and 6–0–6 dual-rotating propellers, in each case for three advance ratios. The potential drop is given in nondimensional form and is plotted against the radius. Each curve represents a radial line on the helix. The angular position of the radial line is given as a fraction of the cell semiangle measured from the middle or symmetry line of the cell.

Figure 18 shows $K(x)$ as the potential difference at the zero angle or midway between two successive intersecting lines. The results are arranged in order showing the four-, eight-, and twelve-blade dual-rotating propellers at three advance ratios.

The function $K(\theta)$ is shown in figure 19 plotted against the angle measured from the same zero reference angle. Results are shown for the same three propellers at the same three advance ratios. Curves are shown for three values of the radial distance $x=\frac{1}{4}, \frac{1}{2}$, and $\frac{3}{4}$.

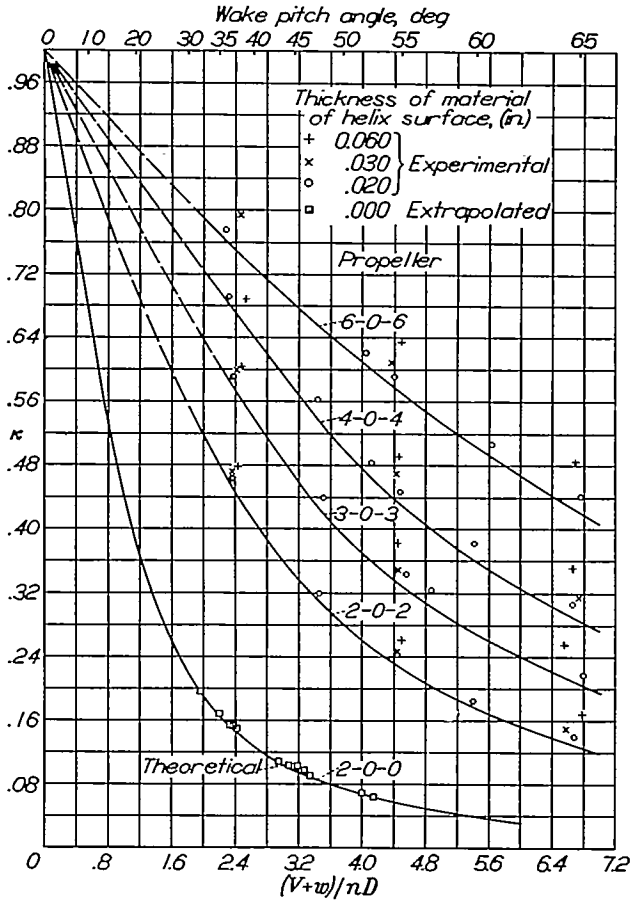

FIGURE 15.—Measured values of mass coefficient κ for dual-rotating propellers with various numbers of blades.

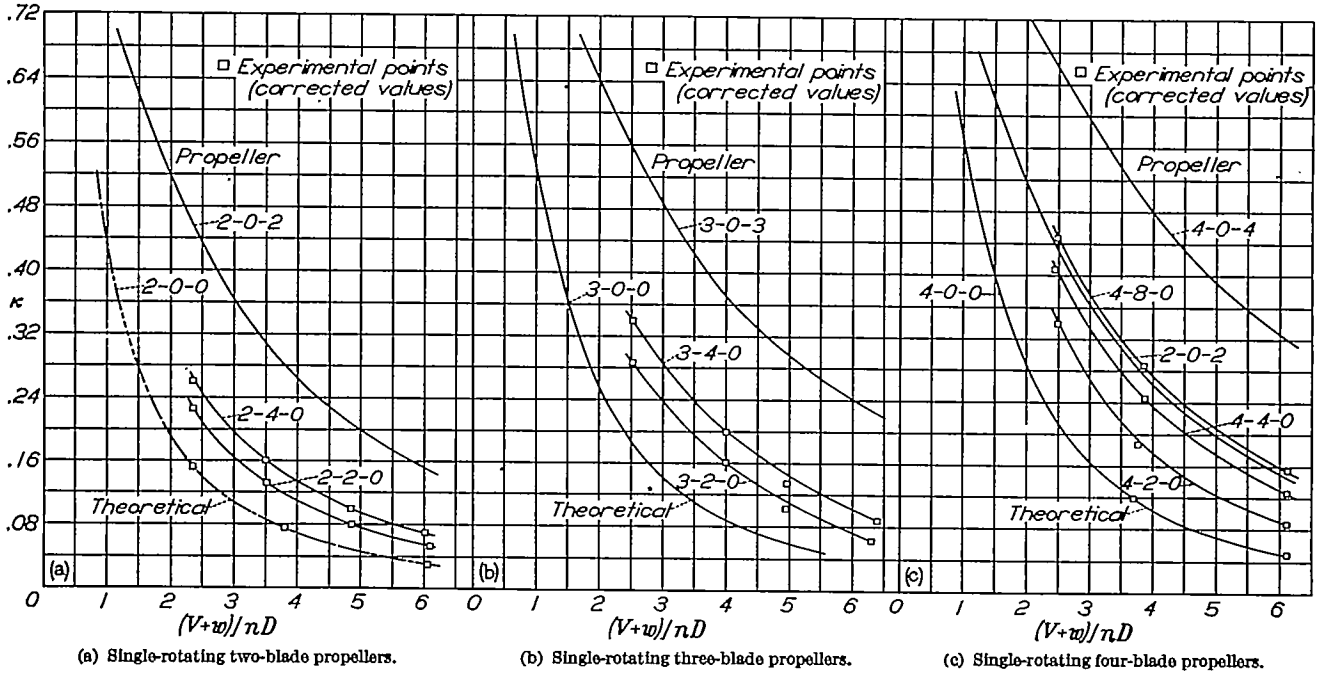

(a) Single-rotating two-blade propellers. (b) Single-rotating three-blade propellers. (c) Single-rotating four-blade propellers.

FIGURE 16.—Measured values of mass coefficient κ against $\frac{V+w}{nD}$ showing the effect of guide vanes.

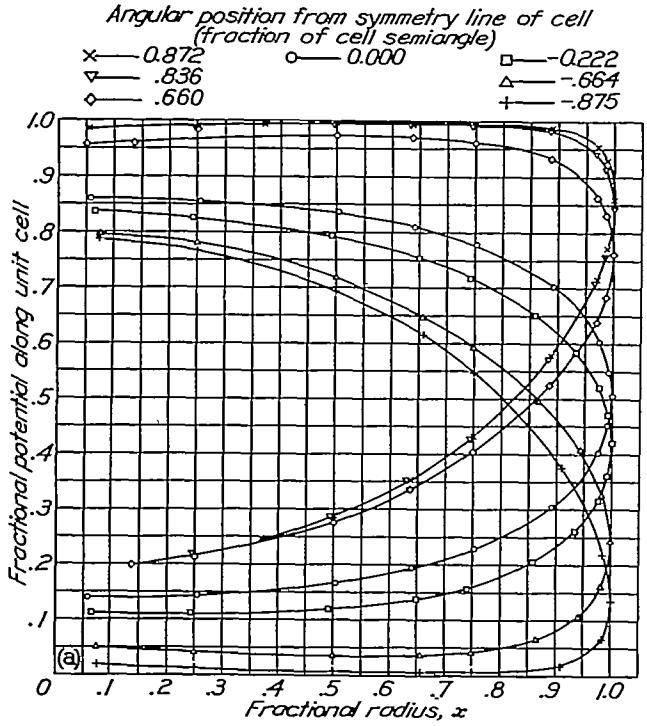

(a) 2-0-2 unit cell; $\frac{V+w}{nD}=1.89$.

FIGURE 17.—Variation of potential along a radius for various angular positions.

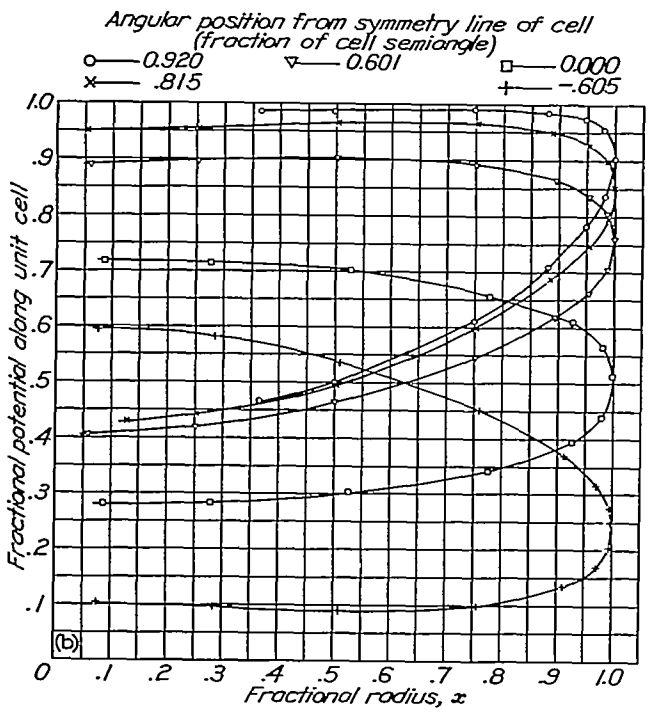

(b) 2-0-2 unit cell; $\frac{V+w}{nD}=3.14$.

FIGURE 17.—Continued.

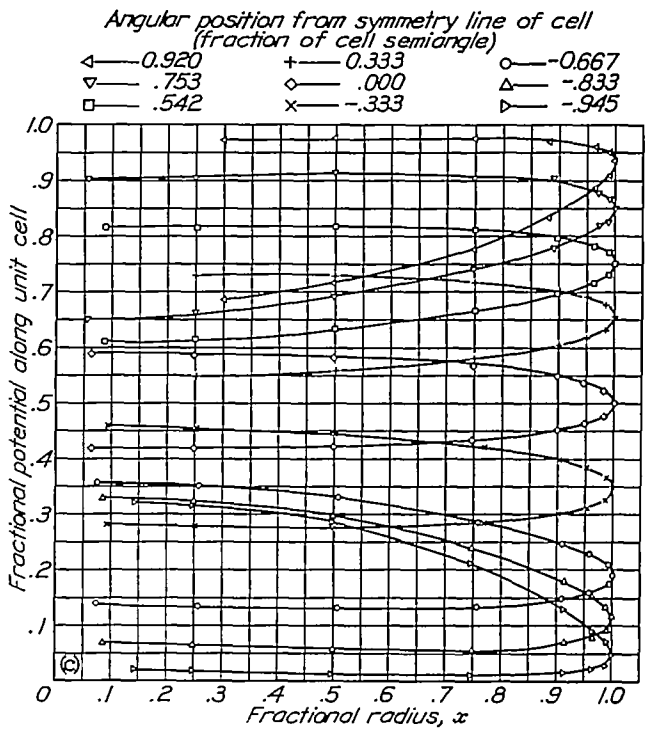

(c) 2-0-2 unit cell; $\frac{V+w}{nD}=0$.

FIGURE 17.—Continued.

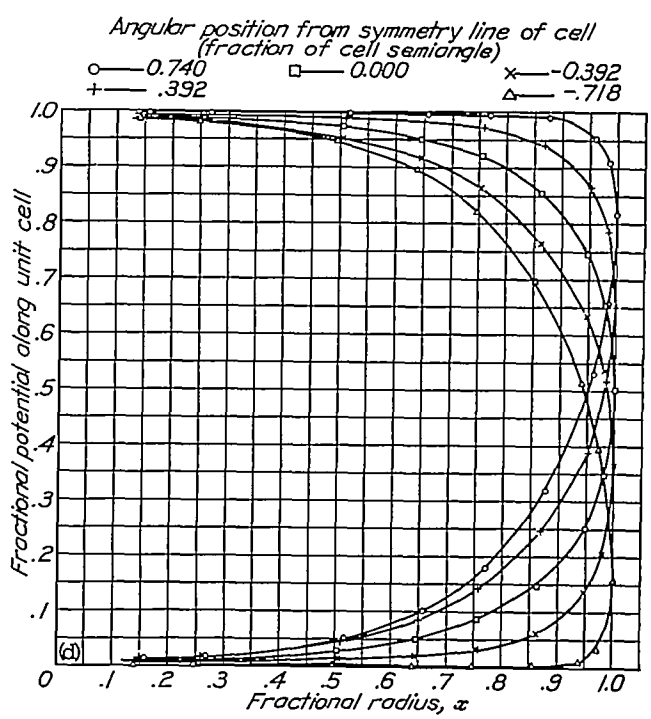

(d) 4-0-4 unit cell; $\frac{V+w}{nD}=1.55$.

FIGURE 17.—Continued.

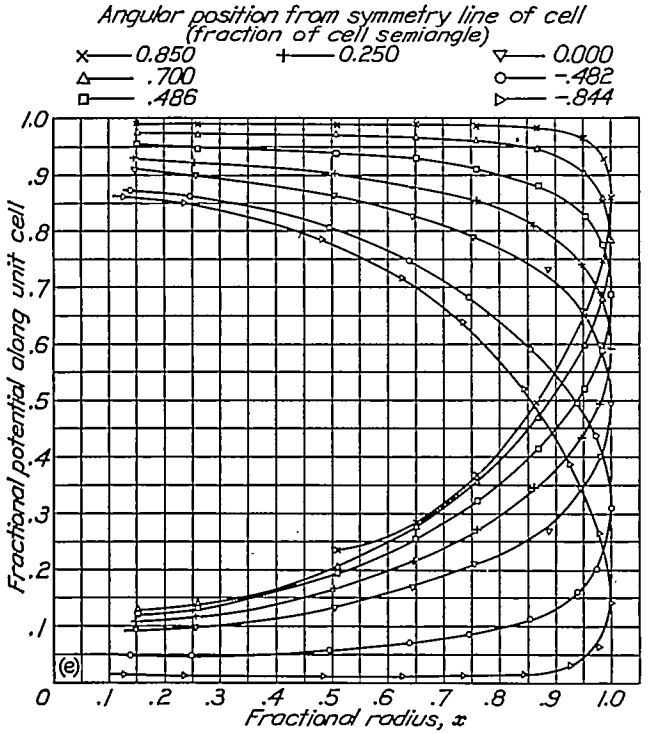

(e) 4-0-4 unit cell; $\frac{V+w}{nD}=3.11$.

FIGURE 17.—Continued

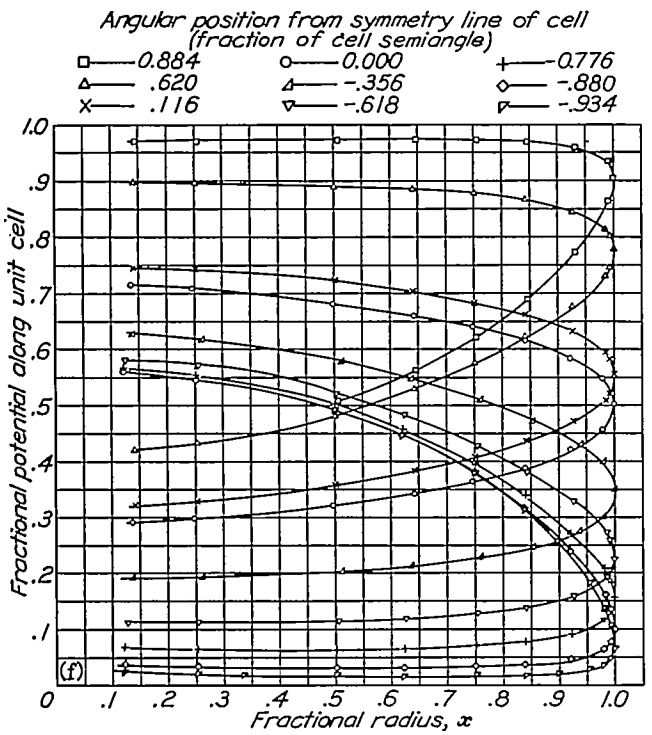

(f) 4-0-4 unit cell; $\frac{V+w}{nD}=6.34$.

FIGURE 17.—Continued.

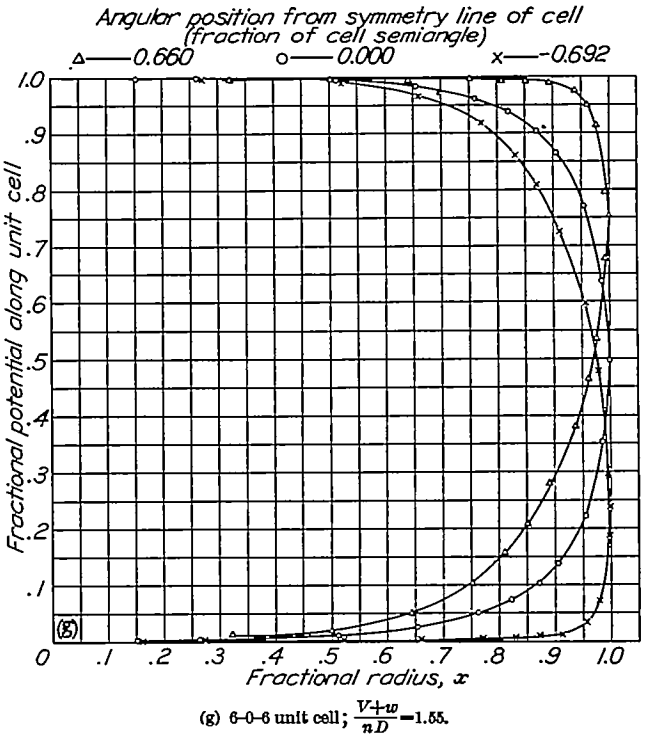

(g) 6-0-6 unit cell; $\frac{V+w}{nD}=1.55$.

FIGURE 17.—Continued.

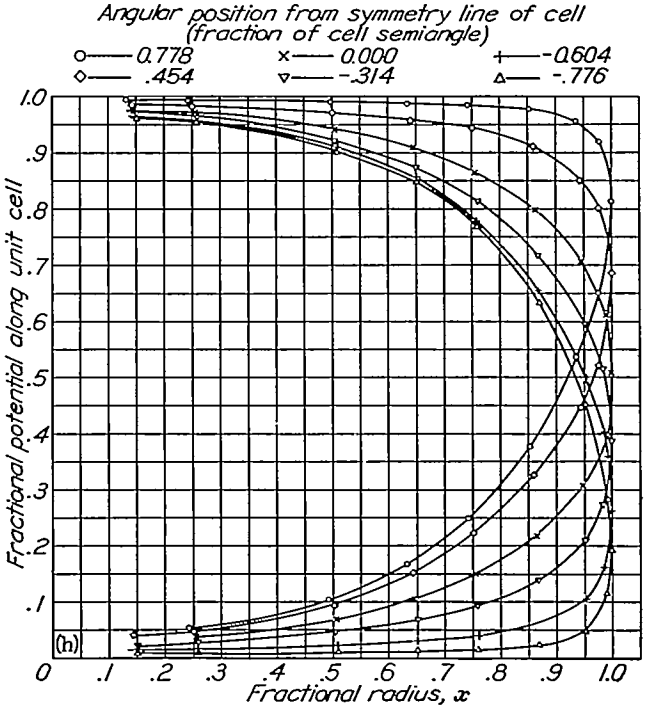

(h) 6-0-6 unit cell; $\frac{V+w}{nD}=3.12$.

FIGURE 17.—Continued

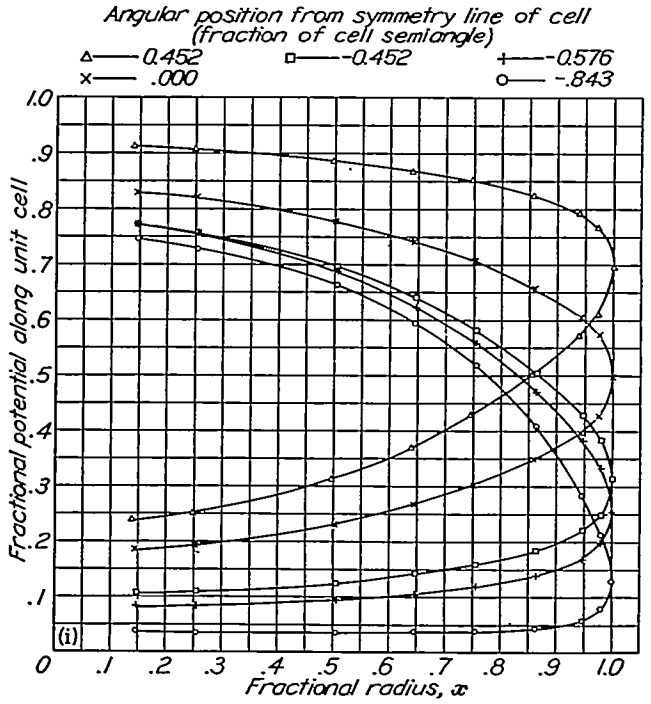

(i) 6-0-6 unit cell; $\frac{V+w}{nD}=6.41$.

FIGURE 17.—Concluded.

DISCUSSION

The concept of a mass coefficient κ defined as

$$\kappa \equiv 2\int_0^1 K(x)x\,dx$$

has been introduced, where $K(x)$ is a nondimensional distribution function and x is the nondimensional radius. Numerical values of κ for the known cases of single-rotating propellers are shown in figure 3. It is noted that the mass coefficient drops rapidly with the advance ratio. For $\frac{V+w}{nD}=2$, the value of κ is less than 0.5 even for an infinite number of blades and is less than 0.2 for the two-blade single-rotating propeller.

For dual-rotating propellers the mass coefficient defined a

$$\kappa=\frac{1}{\pi}\int_0^1\int_0^{2\pi} K(x,\theta)x\,dx\,d\theta$$

is considerably larger. A 2–0–2 propeller has, in fact, a larger mass coefficient at $\frac{V+w}{nD}=2$ than the single-rotating propeller with an infinite number of blades. The 6–0–6 propeller at the same advance ratio has a mass coefficient $\kappa=0.79$ or near unity. (See fig. 15.)

The effect of guide vanes is of considerable practical interest. These vanes are stationary and are arranged either immediately in front of or behind the propeller. The question is whether such a stationary system in some cases may be more acceptable than a dual arrangement of counterrotating propellers. As an example, consider a three-blade single-rotating propeller at an advance ratio of 3. (See fig. 16(b).) The mass coefficient κ of the propeller alone is seen to be 0.142; the 3–2–0 propeller with two guide vanes shows a value of κ of 0.238, and the 3–4–0 propeller with four guide vanes shows a value of κ of 0.286. For comparison, the

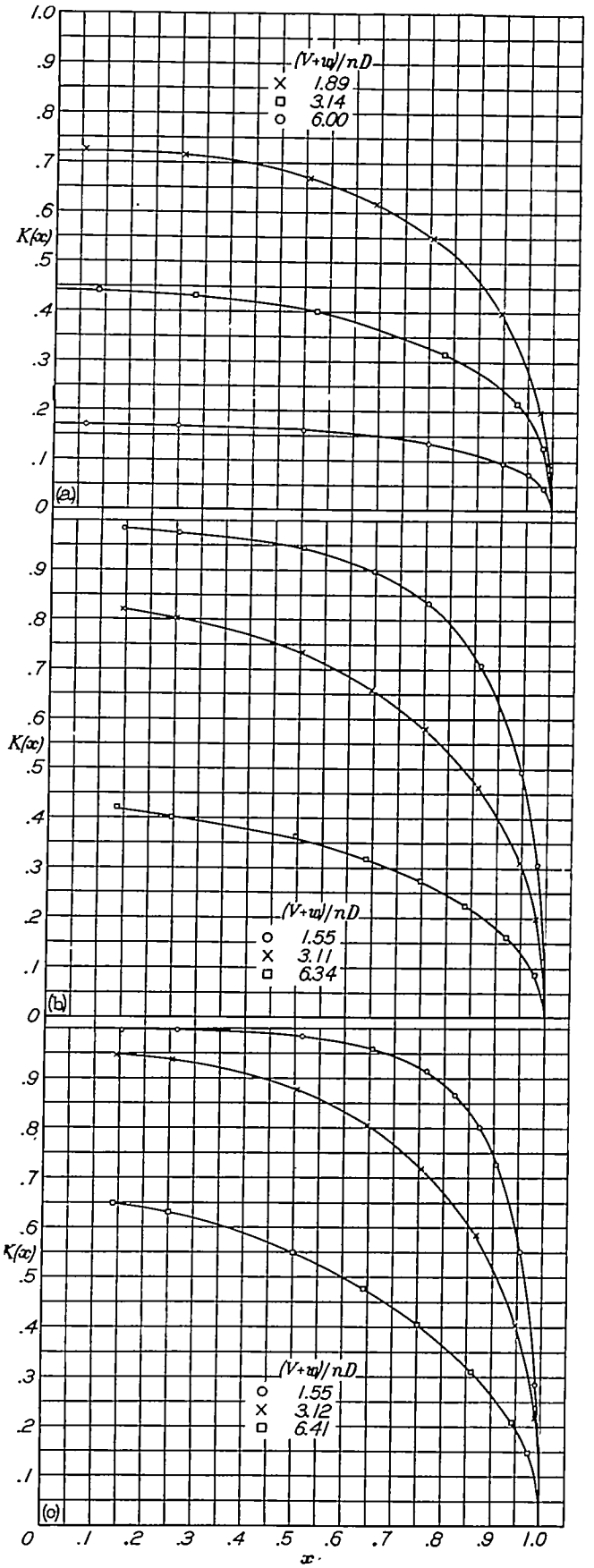

(a) 2-0-2 helix surface.
(b) 4-0-4 helix surface.
(c) 6-0-6 helix surface.

FIGURE 18.—Measured values of the potential difference $K(x)$ on the helix surface taken midway between two successive lines of intersection. (1-ft radius rubber helix section; see figs. 12, 13, and 14.)

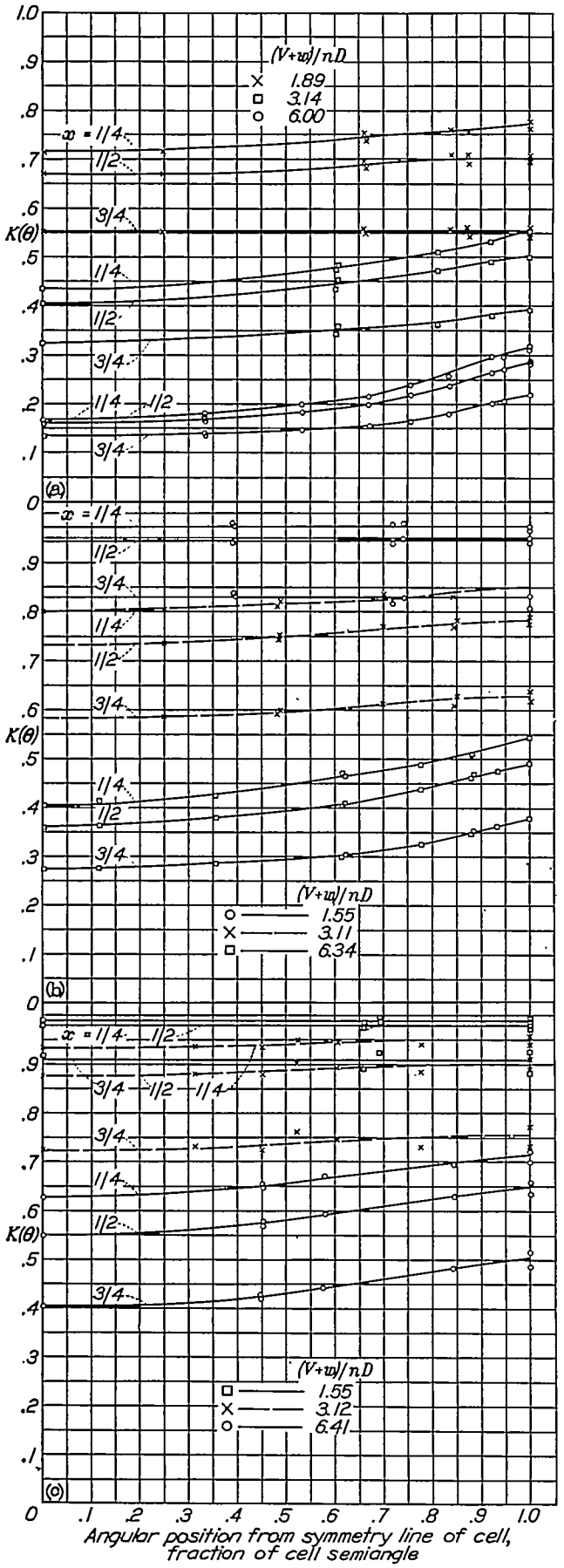

(a) Time function of $K(\theta)$ for 2-0-2 surface.
(b) Time function of $K(\theta)$ for 4-0-4 surface.
(c) Time function of $K(\theta)$ for 6-0-6 surface.

FIGURE 19.—Measured values of the potential difference at various radii and distances along the helix surface.

six-blade dual-rotating propeller shows a value of κ of 0.486 at the same advance ratio. If a dual-rotating propeller is not used, the double guide vane is undoubtedly desirable in some cases. Actually, the induced loss is reduced to about half as compared with the loss in the case without vanes. The difference in the effect of two or four vanes is relatively small.

LANGLEY MEMORIAL AERONAUTICAL LABORATORY,
NATIONAL ADVISORY COMMITTEE FOR AERONAUTICS,
LANGLEY FIELD, VA., *May 27, 1944.*

APPENDIX

SYMBOLS

V	advance velocity of propeller
w	rearward displacement velocity of helical vortex surface (at infinity)
n	rotational speed of propeller, revolutions per second
ω	angular velocity of propeller ($2\pi n$)
D	diameter of vortex sheet
$\frac{V+w}{nD}$	advance ratio of wake helix
$\lambda=\frac{1}{\pi}\frac{V+w}{nD}$	
H	pitch of wake helix $\left(\frac{V+w}{n}\right)$
Γ	circulation at radius r
$K(x)$	circulation function for single rotation $\left(\frac{p\Gamma\omega}{2\pi(V+w)w}\right)$
$K(x,\theta)$	circulation function for dual rotation
p	number of blades of propeller or separate helix surfaces
κ	mass coefficient $\left(2\int_0^1 K(x)x\,dx \text{ or } \frac{1}{\pi}\int_0^1\int_0^{2\pi} K(x,\theta)x\,dx\,d\theta\right)$
x	ratio of radius of element to tip radius of vortex sheet (r/R)
r	radius of element of vortex sheet
R	tip radius of vortex sheet $\left(\frac{1}{2}D\right)$
θ	angular coordinate on vortex sheet
F	projected area of helix (πR^2)
S	area of end plates of cylindrical test tank
I_0	current through test tank with helix removed
ΔI	reduction in current due to presence of helix

REFERENCES

1. Goldstein, Sidney: On the Vortex Theory of Screw Propellers Proc. Roy. Soc. (London), ser. A, vol. 123, no. 792, April 6, 1929, pp. 440–465.
2. Kramer, K. N.: The Induced Efficiency of Optimum Propellers Having a Finite Number of Blades. NACA TM No. 884, 1939.
3. Lock, C. N. H., and Yeatman, D.: Tables for Use in an Improved Method of Airscrew Strip Theory Calculation. R. & M. No 1674, British A. R. C., 1935.